frontiers in Earth Science

ORIGINAL RESEARCH
published: 28 August 2020
doi: 10.3389/feart.2020.00352

Insights Into Magma Chamber Processes From the Relationship Between Fabric and Grain Shape in Troctolitic Cumulates

Marian B. Holness[1], Charlotte Morris[1], Zoja Vukmanovic[1] and Dan J. Morgan[2]*

[1] Department of Earth Sciences, University of Cambridge, Cambridge, United Kingdom, [2] School of Earth and Environment, University of Leeds, Leeds, United Kingdom

The strength of foliations defined by shape preferred orientation of plagioclase in troctolitic cumulates from the Layered Series of the Skaergaard intrusion, and the Rum Eastern Layered Intrusion, increases as the grains become more tabular, due either to the greater propensity of highly non-equant grains to be re-arranged by magmatic currents or tectonic disruption of poorly consolidated mush, or by the effects of a pre-existing shape preferred orientation on final grain shape in fully solidified rocks. The stratigraphic evolution of grain shape, microstructures and fabrics in the lowest 320 m of the Skaergaard Layered Series records the progressive inflation of the chamber to its final size. During the earliest stages of solidification, the extent of *in situ* nucleation and growth on the chamber floor decreased upward through the stratigraphy, due to the development of a thermally insulating blanket of mush on the floor. An upward increase in foliation strength as the chamber inflated to its final size was a result of the increasing strength of convection of the bulk magma and an increasing contribution to the floor mush of crystals derived from the walls of the enlarging magma chamber. Plagioclase in the troctolites in the open-system magma chamber of the Rum Eastern Layered Intrusion is generally more equant than that in the Skaergaard intrusion, perhaps related to the slower crystal growth on the margins of the continuously replenished Rum chamber. Significant sub-solidus modification of original igneous microstructures is observed in Rum troctolites from parts of the stratigraphy recording frequent replenishment events.

Keywords: fabric, cumulate, grain shape, Skaergaard intrusion, Rum (NW Scotland)

OPEN ACCESS

Edited by:
David A. Neave,
The University of Manchester,
United Kingdom

Reviewed by:
Stearns Anthony Morse,
University of Massachusetts Amherst,
United States
Eric C. Ferre,
University of Louisiana at Lafayette,
United States

****Correspondence:***
Marian B. Holness
marian@esc.cam.ac.uk

Specialty section:
This article was submitted to Petrology, a section of the journal Frontiers in Earth Science

Received: *20 January 2020*
Accepted: *29 July 2020*
Published: *28 August 2020*

Citation:
Holness MB, Morris C, Vukmanovic Z and Morgan DJ (2020) Insights Into Magma Chamber Processes From the Relationship Between Fabric and Grain Shape in Troctolitic Cumulates. Front. Earth Sci. 8:352. doi: 10.3389/feart.2020.00352

INTRODUCTION

Fabrics formed by a preferred grain orientation in igneous rocks potentially preserve valuable information about processes occurring during solidification. Here we focus on fabrics defined by a shape-preferred orientation (SPO) of plagioclase in mafic cumulates. Such shape-preferred fabrics were initially thought to result from settling of non-equant grains from a stagnant magma (Hess, 1960; Jackson, 1961) but, following Grout (1918), it has since been strongly argued that fabrics are a consequence of deposition from, or re-working of crystals by, flowing magma or of

tectonic re-working of dis-aggregated mushes (e.g., Wager and Deer, 1939; Brothers, 1964; Wager and Brown, 1968; Higgins, 1991; Vukmanovic et al., 2018): they can therefore be classified as primary or secondary fabrics according to the scheme of Holness et al. (2017). However, there is a considerable literature arguing that all fabrics observed in mafic cumulates form during recrystallisation associated with gravitationally driven compaction of relatively melt-poor crystal mushes (e.g., Young and Donaldson, 1985; Boudreau and McBirney, 1997; Boorman et al., 2004): these are the tertiary fabrics of Holness et al. (2017). These two fabric-forming mechanisms can be differentiated using evidence for recrystallisation during deformation, by the spatial distribution of any compositional zoning, from the relationship between the SPO and any crystallographic-preferred orientation (CPO), and by a direct assessment of the extent of deformation by either dislocation creep or dissolution-reprecipitation (Holness et al., 2017).

In this contribution we concentrate on fabrics formed by crystal re-arrangement in melt-rich environments and demonstrate how detailed examination of the relationship between plagioclase grain shape and grain orientation, as viewed in thin section, provides information about the thermal history of a magma body. We show how microstructures can be used to demonstrate the progressive decrease in heat loss through the chamber floor during the early history of a deep, closed-system, magma chamber. We also assess the importance of sub-solidus microstructural modification by textural equilibration. By concentrating on samples with the same primocryst assemblage (troctolitic cumulates) we reduce the number of variables that might be controlling the microstructure.

PREVIOUS WORK

Grain Shape

Despite recent advances in 3D tomographic techniques (e.g., Denison et al., 1997; Jerram et al., 2010), the most accessible way to determine grain shape in rocks dominated by a single mineral remains microscopic examination of thin sections. However, thin sections provide a 2D slice through 3D material, introducing uncertainty in the true 3D shape or range of shapes present in a rock. Progress has been made by computing the range of shapes of grain intersections expected for an idealized shape (Higgins, 1994; Morgan and Jerram, 2006), calculated for the two endmembers of completely random orientations and an entirely foliated fabric (Higgins, 1994). The grains in real rocks, however, are likely to have a range of shapes (Duchêne et al., 2008), requiring a more sophisticated treatment involving the determination of the crystallographic orientation of each grain (Farr et al., 2018).

The shape of plagioclase grains is a sensitive function of cooling and crystallization rates (Lofgren, 1974; Sato, 1995). At cooling rates typical of dolerites and gabbros, Ca-rich plagioclase growth is interface-controlled: unimpeded growth results in tabular grains with the large faces parallel to (010). The tablets may be elongated along the *c*-axis but are more commonly elongate along the *a*-axis (see discussion in Smith and Brown, 1988). Holness (2014) demonstrated that in mafic rocks in which the plagioclase grains are randomly oriented, the arithmetic mean, or average, apparent aspect ratio as viewed in thin section, AR [a parameter also used by Meurer and Boudreau (1998) and Boorman et al. (2004)], is a function of cooling rate: the slower the cooling, the lower the value of AR. This method of quantifying grain shape is independent of the range of shapes present in the rock.

Fabrics in Igneous Rocks

The classification scheme of Holness et al. (2017) divides igneous fabrics into three categories: primary (formed during crystal nucleation and growth, or during accumulation of crystals mobilized by gravity or magmatic currents); secondary (forming post-accumulation, during slumping or mechanical re-arrangement of crystal-rich material in the transition between suspension flow and solid state); and tertiary (formed by recrystallization of low-porosity mush). In order to decode magmatic behavior, we must therefore exclude rocks with tertiary fabrics.

Tertiary fabrics, formed in low-porosity mush, require grains to change shape during plastic deformation. Plastic deformation by dislocation creep leaves a clearly identifiable microstructural signature. Tertiary fabrics may also form during plastic deformation by pressure solution mechanisms, potentially leaving clues in the spatial distribution of compositional zoning (Svahnberg and Piazolo, 2013). However, the commonly observed relationship between SPO and CPO in mafic igneous rocks solidified in tectonically inactive regions (i.e., the long, short and intermediate axes of the plagioclase grains are generally oriented in the same way relative to the crystal structure) can only occur if there is anisotropy of either dissolution, precipitation (e.g., Svahnberg and Piazolo, 2013) or grain boundary sliding (Miyazaki et al., 2013). Although little is known about anisotropy of plagioclase behavior in the super-solidus, in hydrous sub-solidus systems the anisotropy of dissolution is such that it would result in grain elongation perpendicular to the (010) faces (Heidelbach et al., 2000; Arvidson et al., 2004; Svahnberg and Piazolo, 2013). Plagioclase in mafic cumulates is almost invariably tabular parallel to (010), as is that grown as isolated grains in melt, suggesting that cumulate SPO fabrics are highly unlikely to be tertiary dissolution-reprecipitation fabrics.

Shape-preferred orientation fabrics formed during *in situ* nucleation and growth at the magma-mush interface (i.e., involving no grain mobilization) are confined to systems in which grain growth is controlled by steep gradients in either composition or temperature, leading to comb layering defined by the growth of elongate grains along the gradient. Examples include the harrisites of Rum (Donaldson, 1974), spinifex-textured olivine in komatiite flows (*ibid.*), and the perpendicular feldspar rock of Skaergaard (Wager and Deer, 1939). If, however, the temperature and/or compositional gradients driving crystallization are shallow, *in situ* crystal nucleation and growth does not result in fabric formation: instead, grains nucleate with random orientations and grow until they impinge against adjacent grains. The dominance of heterogeneous nucleation on pre-existing grains is likely to create a strongly cohesive mush

which cannot undergo the extensive disaggregation necessary for grain re-arrangement and secondary fabric formation.

Thus, microstructures formed during *in situ* nucleation and growth with no subsequent mobilization of grains, and in the absence of strong compositional or temperature gradients, are characterized by the absence of an SPO. They are furthermore characterized by the prevalence of irregular grain boundaries that are not generally parallel to expected growth faces, by the presence of small mineral inclusions on the irregular grain boundaries [termed "impingement lenses" by Holness et al. (2007a)], by a wide range of grain sizes indicative of an extended nucleation period and the absence of hydrodynamic sorting (Holness et al., 2019), by the absence of any correlation between the location of compositional zoning and crystallographic orientation, and by the presence of partially included grains of the same phase as the enclosing grain (Holness et al., 2019) (**Figure 1a**). Within a group of samples from the same body, the average apparent aspect ratio of plagioclase will have a negative correlation with the median value of the clinopyroxene-plagioclase-plagioclase dihedral angle, Θ_{cpp} (Holness, 2015). Any oikocrysts enclose chadacrysts of a wide range of sizes (McBirney and Hunter, 1995) (**Figure 1a**).

Conversely, primary and secondary fabrics are commonly created by grain alignment during mobilization, transport and accumulation of crystals grown elsewhere. The strength and nature of fabrics formed by grain re-arrangement in a current are a function not only of grain shape, but also depend on particle concentration and the extent to which particles interact during transport (Rust, 1972; Mainprice and Nicolas, 1989; Iso et al., 1996; Yamamoto and Matsuoka, 1996). In high Reynolds number systems typical of sedimentary rocks, elongate clasts can be either aligned parallel to the shear direction (Rust, 1972; Davies and Walker, 1974; Yamamoto and Matsuoka, 1996), or aligned parallel to the vorticity axis and perpendicular to the flow direction (Rust, 1972; Iso et al., 1996; Yamamoto and Matsuoka, 1996). A different behavior may pertain, however, in igneous systems in which grains are cohesive and the particle Reynolds number is much lower, but little is known about this.

Rocks with SPO fabrics formed by significant mass transport and crystal re-distribution are characterized by distinct microstructural features. They contain abundant euhedral grains bounded by growth faces, and grain boundaries are commonly planar and formed by the juxtaposition of euhedral grains (**Figure 1b**). Grain boundaries defined by the juxtaposition of planar growth faces are not commonly associated with compositional zoning, which is instead confined to crystal margins adjacent to interstitial phases (unless, of course, the grains were zoned before they were brought into contact during re-distribution). There is no correlation between overall plagioclase grain shape and Θ_{cpp} (Holness, 2015). There may be a rather narrow range of grain sizes, indicative of hydrodynamic sorting before accumulation.

It is important to note here that cumulates formed by re-distribution of crystals grown elsewhere may have no fabric if the accumulated grains were not given a preferred orientation either during primary deposition or by re-working, or if the accumulation was formed of poorly packed grain clusters (Jackson, 1961; Campbell et al., 1978). Such accumulations might acquire a (secondary) fabric if the framework collapses during compaction (pure shear) as a consequence of gravitational loading (Gray et al., 2003; Philpotts and Philpotts, 2005), during slumping (simple shear) of an unstable crystal pile (e.g., O'Driscoll et al., 2007), or by seismically induced fluidization (e.g., Davis et al., 2007; Bergantz et al., 2017). Although theoretical models suggest there is no fixed volume fraction representing lock-up if the crystal mush is subjected to shearing during,

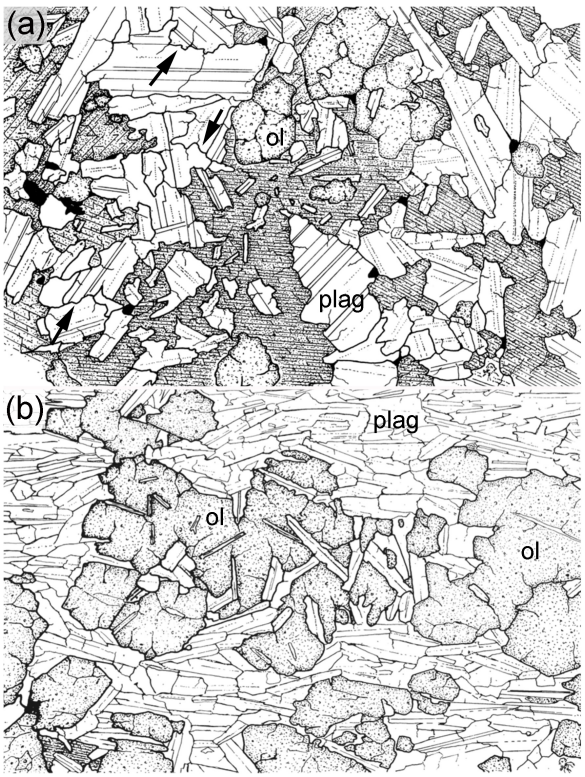

FIGURE 1 | Line drawings of troctolitic cumulates, reproduced with permission from Journal of Geology, from McBirney and Hunter (1995). The cleavage of pyroxene and the twinning of plagioclase are idealized, olivine is stippled and the opaque phase is Fe-Ti oxide. No scale bars were provided in the original drawings, but this absence does not detract from the value of the images, in which the (scale-invariant) grain shape, size distribution, and morphology of grain boundaries are the main points of interest. **(a)** Troctolitic cumulate from LZa of the Skaergaard, with poikilitic interstitial pyroxene, and a microstructure indicative of *in situ* nucleation and growth. Note the absence of a shape preferred orientation of the plagioclase, the wide range of grain sizes (pointing to a prolonged period of nucleation, with no hydrodynamic sorting), and the irregular grain boundaries commonly at high angles to expected growth faces typical of growth to impingement (examples are arrowed). In such rocks, minerals commonly have compositional zoning adjacent to interstitial grains (not shown). **(b)** A troctolite from the Eastern Layered Series of Rum, with the expected microstructure for a crystal mush formed predominantly by the accumulation of crystals grown elsewhere. The strong lamination is defined by a shape preferred orientation of euhedral, unzoned, plagioclase. Grain boundaries are generally planar, formed by juxtaposition of euhedral grains bounded by growth faces. The narrow range of grain sizes is consistent with hydrodynamic sorting. Plagioclase grains enclosed by olivine are generally more elongate and randomly oriented, preserving an early stage of mush history.

e.g., seismic activity, slumping due to slope instability, magma re-injection or bubble nucleation (e.g., Petford and Koenders, 2003; Petford, 2009; Bergantz et al., 2017; Petford et al., 2020), secondary fabrics can only form by such mechanisms if the mush does not contain sufficient strong grain boundaries to prevent disaggregation. Philpotts et al. (1996) find there is only a limited window at ∼33 vol.% solid for secondary fabric formation by gravitational loading of a basaltic mush in bodies of ∼100 m height: the mush clearly becomes too strong at lower porosities to permit disruption by gravitational loading alone.

If randomly oriented accumulations retain their high initial porosity [e.g., if the grain population is dominated by elongate or highly tabular grains which do not pack efficiently at random orientations (Williams and Philipse, 2003)], the final microstructure might be difficult to distinguish from one created entirely by *in situ* nucleation and growth as the only points of difference might be the absence of a wide range of grain sizes, the absence of partially included grains of the same phase, and the lack of intrusion-scale correlation between overall plagioclase grain shape and Θ_{cpp}.

Reported Examples of the Relationship Between Fabric and Grain Shape

Fabric strength and grain shape are commonly positively correlated in cumulates. A strong relationship between fabric and the shape of feldspars is found in the alkaline layered intrusions of the Gardar Province, South Greenland, in which foliation formed by a feldspar SPO is almost perfect in nepheline syenites containing wafer-thin alkali feldspar grains, but is weak or absent in syenitic cumulates containing almost equant feldspar (Upton et al., 1996). Since the packing of the feldspars in the latter is highly inefficient compared to that in the former, this relationship leads to an associated correspondence between modes of interstitial phases and the fabric strength.

Higgins (1991) found that the plagioclase in a sample of laminated anorthosite from the Sept Iles intrusion was less equant than that in a sample of closely associated massive anorthosite from the same intrusion. Followed by Higgins and Chandrasekharam (2007); Higgins (1991) attributed the difference to changes in the chemical potential gradient in the liquid surrounding the growing crystals, citing Kouchi et al. (1986) to argue that the less equant crystals in the laminated anorthosite were a consequence of them growing from relatively strongly flowing magma. However, Kouchi et al. (1986) demonstrated that, at any given undercooling, crystals in a stirred liquid grow with shapes indicative of a smaller undercooling of a static liquid, i.e., the transition from interface-controlled growth to diffusion-limited growth requires a greater undercooling in stirred, compared to static, liquid. Since plagioclase becomes less equant as the undercooling is increased (e.g., Shea and Hammer, 2013), the relatively less equant crystals in the laminated anorthosite are unlikely be a consequence of magma flow.

Meurer and Boudreau (1998) also report a positive correlation between foliation strength and plagioclase shape in plagioclase-rich cumulates (anorthosites, troctolites, and gabbros) from the Stillwater Complex, Montana. However, they argue that it was caused by recrystallisation during gravitationally driven compaction [i.e., a tertiary fabric according to the scheme of Holness et al. (2017)]. In agreement with Boudreau and McBirney (1997), Holness et al. (2017) pointed out that such a hypothesis requires a strong anisotropy of dissolution in plagioclase perpendicular to that seen in hydrous systems (Heidelbach et al., 2000; Arvidson et al., 2004; Svahnberg and Piazolo, 2013). Demonstration of fabric formation by recrystallization during compaction is possible using careful microstructural examination, since it would result in the truncation of both original growth faces and intra-crystalline compositional zonation in rocks dominated by the accumulation of crystals grown elsewhere: no evidence has yet been presented in support of this.

Modification of Grain Shape in the Sub-Solidus

Microstructures formed during crystal growth from a melt may be modified subsequently during either super- or sub-solidus textural equilibration driven by the minimization of interfacial energies. Such equilibration can result in the loss of primary grain shape and SPO, and the truncation of any concentric compositional zoning formed during solidification. A close approach to textural equilibrium results in smooth grain boundary curvature (and hence rounding of planar growth faces and the attainment of equant grain shapes), the establishment of equilibrium dihedral angles at the corners of any melt-filled pores and at all three- and four-grain junctions, and grain growth. Textural equilibration is fastest in the super-solidus (Ikeuye and Smith, 1949), but in the sub-solidus is fastest in monomineralic domains, where it involves only grain boundary migration, rather than diffusion along grain boundaries (Hunter, 1996).

The first stage of textural equilibration is the attainment of the equilibrium geometry in the immediate vicinity of all melt–solid–solid and three- and four-grain junctions. The relatively slow rate of sub-solidus equilibration at poly-phase junctions means that the geometry of clinopyroxene-plagioclase-plagioclase three-grain junctions is generally unmodified in gabbros from all layered intrusions investigated to date (e.g., Holness et al., 2012), whereas this is not expected to be the case for three-grain junctions involving only one phase (i.e., monomineralic junctions). Further progression of sub-solidus textural equilibration involves grain boundary migration as all interfaces attain constant mean curvature, creating a granular microstructure with equant grains. The final stage of equilibration involves grain growth by a combination of Ostwald ripening in poly-mineralic domains and normal grain growth in monomineralic domains. Textural equilibration therefore results in a reduction in average apparent aspect ratio, the loss of SPO fabrics, and an increase in grain size. Note, however, that the crystallographic orientation of individual grains remaining after grain growth (and therefore any CPO fabric) remains essentially unchanged, providing the opportunity to detect the presence of an original magmatic SPO.

For rocks which have undergone only the minimal amount of textural equilibration (i.e., they retain the original igneous

geometry of both two-phase three-grain junctions and grain boundaries) the only indication of sub-solidus textural equilibration will be found in the geometry of three-grain junctions in monomineralic domains. Although the median and average value of the dihedral angle at junctions between three grains of the same mineral are necessarily 120°, regardless of the extent to which equilibrium has been approached, any textural equilibration will be recorded by a change in the standard deviation of the population of dihedral angles (Kretz, 1994).

For monomineralic systems in which there is no anisotropy of interfacial energies, the standard deviation of a population of dihedral angles is zero. However, all minerals of geological interest are anisotropic to some extent, so a fully texturally equilibrated microstructure has a finite value of standard deviation of dihedral angle populations (Kretz, 1966). For example, the standard deviation of a population of plagioclase–plagioclase–plagioclase junctions in a high-grade metamorphic rock presumed to be in, or very close to, textural equilibrium is in the range 9.1–13° (Vernon, 1968, 1970). Little is known about the likely range of dihedral angles in monomineralic silicates that have undergone no sub-solidus equilibration. Elliott et al. (1997) created artificial 3D microstructures by permitting randomly positioned grains to grow to impingement and found that the population of dihedral angles measured in 2D slices through the fully solidified 3D aggregate was similar to that expected for one with a standard deviation of 20° of the true 3D dihedral angles. However, these artificial microstructures did not include the effects of growth anisotropy: plagioclase grows as facetted grains, commonly leading to the high-angle impingement of grain boundaries against planar (010) plagioclase faces in gabbros with no fabric (e.g., Kretz, 1966; Vernon, 1968). We might thus expect a standard deviation >20° for populations of plagioclase–plagioclase–plagioclase dihedral angles in unequilibrated igneous rocks containing randomly oriented plagioclase.

A Regime Diagram

Any correlations between grain shape and the strength of primary igneous SPO fabrics result from a complex interplay of two-way interactions between shape and fabric in a liquid-rich environment. The microstructures resulting from super-solidus processes may then be modified in the sub-solidus during textural equilibration. These interactions can be illustrated using a simple regime diagram (**Figure 2**) relating the average apparent aspect ratio, AR, to the alignment factor, AF, for which a value of 100 denotes perfect alignment to form a foliation and one of 0 denotes perfectly random orientation.

Particle shape affects fabric strength because highly non-equant particles will be more strongly aligned by magmatic currents than more equant particles. Conversely, the extent to which non-equant grains are aligned in a solidifying mush can affect grain shape as solidification progresses, since growth cannot occur on the faces of crystals in contact with their neighbors. This means that crystals in an accumulation with an original SPO fabric [e.g., an accumulation of tabular plagioclase crystals predominantly touching on their (010) faces] will become increasingly non-equant with continued solidification since they can only grow on faces adjacent to melt (Brown, 1956). In this case, the early development of an SPO controls the final shape of the constituent grains, resulting in a decrease in the slope of a positive correlation between AF and AR created by current action (**Figure 2A**). [As an aside, this effect of fabric on final grain shape means that AR in a foliated dolerite or gabbro cannot be mapped straightforwardly onto cooling rates in the way it can be for those with randomly oriented plagioclase (Holness, 2014)].

As a consequence of this two-way interaction, for the simplest case in which particles can assume any shape, we would expect a positive correlation between AF and AR, with a zero value of AF (perfect random orientation) for equant grains (AR = 1), and a slope dependent on the balance between the effects of grain rotation by currents and post-accumulation overgrowth (**Figure 2B**). For the particular case of minerals of geological

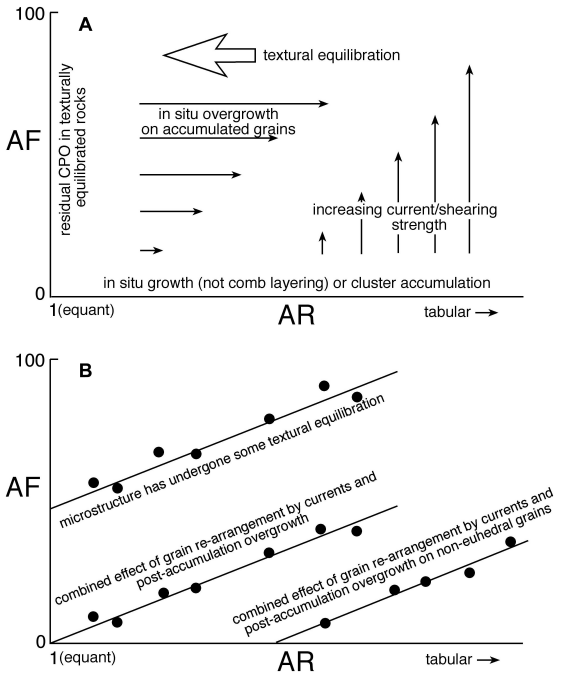

FIGURE 2 | Schematic diagrams of the relationship between fabric strength defined by a shape preferred orientation (SPO, quantified by the alignment factor, AF, which has a value of 0 for randomly aligned grains and a maximum value of 100 for perfectly aligned grains) and the average apparent aspect ratio (AR). **(A)** Rocks with no preferred shape orientation (AF = 0) form predominantly during *in situ* nucleation and growth, or by the accumulation of grain clusters. Positive correlations between alignment factor (AF) and average apparent aspect ratio (AR) can be achieved in two ways: firstly, an increasing fabric strength in a melt-bearing mush results in an increased AR during subsequent solidification, since no growth can occur on faces in contact with other grains (Brown, 1956); secondly, for any given strength of current, particles with higher AR will be re-arranged and aligned to form a stronger preferred alignment. Rocks with entirely equant grains (AR = 1), but with a residual SPO recorded by a crystallographic preferred orientation (i.e., with AF > 0 if defined using CPO), must have undergone extensive textural equilibration. **(B)** Positive correlations between alignment factor (AF) and average apparent aspect ratio (AR) pass through the origin for systems in which particles are free to take any primary shape. Those passing through the *y*-axis must have undergone some textural equilibration, whereas those cutting the *x*-axis are realistic for natural systems in which any mineral grain has a limited range of shapes.

TABLE 1 | Details of troctolitic samples from the Cambridge 1966 drill core through the lower part of the Skaergaard Layered Series.

Sample	Height (m)	Zone	Mineral modes (vol.%)					AR average	AR min	AR max	Plag average length (mm)	AF	Number of grains	Bulk P_2O_5 (wt.%)
			Plag	Ol	Fe-Ti Oxides	Augite	Ca-poor pyroxene							
115′ 9″	163.8	LZa	45.4	36.3	1.6	10.7	6.0	3.10	3.03	3.19	1.408	49.33	213	
211′ 11″	134.4	LZa	74.9	11.0	0.4	10.1	3.6	3.21	3.13	3.29	1.292	53.53	289	0.13
317′ 6.5″	*102.2*	*LZa*	*67.3*	*14.3*	*0.7*	*10.0*	*6.7*	*3.30*	*3.23*	*3.37*	*1.326*	*55.79*	*311*	
351′ 7″	91.8	LZa	67.6	12.5	0.7	14.6	4.6	3.10	3.03	3.17	1.089	47.27	265	0.11
371′ 7″	*85.7*	*LZa*	*71.8*	*18.9*	*0.3*	*6.2*	*2.8*	*3.03*	*2.95*	*3.10*	*0.942*	*55.63*	*451*	*0.12*
438′ 4″	65.4	LZa	65.1	16.3	0.5	14	4.1	3.34	3.25	3.41	1.087	59.64	332	0.11
481′ 1″	52.4	LZa	59.4	18.9	0.8	14.2	6.7	3.06	2.91	3.25	1.302	51.66	251	0.11
511′ 10″	43.2	LZa	65.0	20.5	0.7	9.9	3.9	3.18	3.09	3.26	1.133	56.03	332	0.13
522′ 1″	39.9	LZa	66.9	20.3	0.4	9.6	2.8	3.37	3.30	3.44	1.368	70.88	252	0.08
571′ 4″	24.8	LZa	88.3	5.5	1.2	2.0	3.0	2.81	2.74	2.85	0.933	39.93	323	0.14
621′ 2″	9.7	LZa	74.1	7.5	0.2	15.6	2.7	2.65	2.49	2.78	0.889	39.85	384	0.08
651′ 2″	*0.5*	*LZa*	*74.8*	*12.9*	*0.9*	*7.7*	*3.7*	*2.84*	*2.77*	*2.91*	*1.076*	*40.31*	*303*	*0.08*
671′1 ″	−5.5	HZ	74.1	19.0	0.9	4.9	1.1	2.47	2.41	2.53	0.616	35.29	338	0.04
681′ 1″	−8.6	HZ	57.6	36.6	1.3	2.8	1.7	2.48	2.43	2.54	0.706	55.31	377	0.04
730′ 9″	−23.7	HZ	79.0	10.6	0.7	6.5	3.2	3.09	3.02	3.17	0.987	47.89	381	0.18
760′7 ″	−31.56	HZ	76.3	7.0	2.3	12.4	2.0	2.83	2.69	2.96	0.862	34.51	296	0.09
800′5 ″	−45.0	HZ	76.3	11.7	0.0	9.0	3.0	2.80	2.65	2.94	0.977	30.60	271	0.09
842′ 3″	−57.7	HZ	71.8	14.1	3.7	7.1	3.3	2.44	2.38	2.50	1.047	28.94	280	0.13
867′ 3″	−65.3	HZ	29.8	54.7	2.0	12.9	0.6	2.29	2.23	2.35	0.692	29.96	301	0.13
887′10 ″	−71.6	HZ	77.0	12.7	2.7	4.0	3.6	2.82	2.67	2.90	1.017	31.89	285	0.13
930′2 ″	−84.5	HZ	80.6	8.0	1.7	6.7	3.1	2.53	2.42	2.66	1.191	29.60	220	0.16
933′	−85.4	HZ	77.9	8.6	0.3	3.8	9.4	2.63	2.50	2.74	1.129	17.35	241	0.13
940′6 ″	−87.7	HZ	67.7	21.8	0.4	7.5	2.7	2.56	2.44	2.66	0.943	25.85	227	0.05
979′ 11″	*−99.7*	*HZ*	*62.8*	*25.4*	*0.5*	*7.7*	*3.6*	*2.95*	*2.89*	*3.02*	*0.919*	*33.92*	*320*	*0.10*
987′ 11″	*−102.1*	*HZ*	*70.4*	*12.2*	*0.4*	*15.1*	*1.9*	*2.79*	*2.73*	*2.85*	*1.020*	*35.82*	*338*	
1060′ 1″	−124.1	HZ	72.6	15.3	0.9	5.8	5.4	2.81	2.72	2.86	0.921	21.35	346	0.17
1091′6″	−133.7	HZ	70.9	3.8	0.3	23.8	1.2	2.57	2.52	2.62	1.107	15.03	245	0.06
1122′4 ″	−143.1	HZ	71.0	5.7	2.1	17.6	3.6	2.25	2.14	2.35	0.972	8.10	177	0.09
1145′2 ″	−150.1	HZ	77.0	2.7	3.7	5.6	11.0	2.31	2.20	2.41	0.964	12.82	171	0.10

The sample number gives the depth in feet and inches in the core. HZ, Hidden Zone; LZa, Lower Zone a. Bulk rock P_2O_5 data are from Holness et al. (2015). Mineral modes are either from Holness et al. (2015) or determined as part of the present study. Those samples in italics are those for which AR was previously reported by Holness (2015).

interest, it is rare for grain shape in a suite of related rocks to range from perfectly equant to highly non-equant, so any positive correlation is likely to cut the *x*-axis in **Figure 2B** at some value higher than 1. For the case of plagioclase, the lowest value of AR is likely to be found in those members of a sample suite in which growth was predominantly *in situ* and at random orientations, or in the slowest-cooled members of a sample suite. If the positive correlation between AF and AR cuts the *y*-axis [i.e., a finite value of AF (defined in this case by a CPO, rather than an SPO) is seen when AR = 1], the original microstructure must have been modified by sub-solidus textural equilibration (**Figure 2B**).

CHOICE OF SAMPLES

The Skaergaard Intrusion, East Greenland

The Skaergaard Intrusion formed from the injection of a large (8 km × 11 km × 4 km, Nielsen, 2004) body of relatively evolved tholeiitic basaltic magma into a fault-bounded (Irvine et al., 1998) space forming on the extending margin of East Greenland during the opening of the North Atlantic Ocean, at the unconformity between underlying Precambrian gneisses and an overlying sequence of Eocene plateau lavas (Wager and Deer, 1939). Once the chamber had been filled by a series of magma pulses (Holness et al., 2007b, 2015) it remained closed both to further magma replenishment and to eruption, crystallizing inward from the margins to form one of the world's best examples of progressive fractionation of a basaltic magma.

The least evolved cumulates on the floor of the chamber are troctolitic, forming the Hidden Zone (HZ) and Lower Zone a (LZa) of the Layered Series (Wager and Deer, 1939): they contain primocrysts of olivine and plagioclase with interstitial clinopyroxene, Ca-poor pyroxene (inverted pigeonite), Fe-Ti oxides, apatite and minor quartz, K-feldspar and biotite. The top of LZa, and base of Lower Zone b (or LZb), is marked by clinopyroxene joining the liquidus assemblage. Holness (2015) demonstrated that the average apparent aspect ratio of plagioclase

changes systematically through the Layered Series, with a weakly defined increase in AR through the lowest 950 m, and a well-defined decrease through the overlying stratigraphy to a minimum at ∼2,400 m stratigraphic height.

We chose 29 troctolites from the Cambridge 1966 drill core which covers the lowest 350 m of the floor cumulates, including 150 m of HZ (described in Holness et al., 2015), avoiding samples with strongly poikilitic interstitial pyroxene. In the drill core, the base of LZb is ∼180 m above the top of HZ. Mineral modes are reported in **Table 1**. Bulk rock geochemical analyses of 26 of our samples are reported by Holness et al. (2015). The stratigraphic positions of the samples are shown in **Figure 3** (the zero point of the stratigraphy in this figure is the base of the current exposure, i.e., the division between HZ and LZa). Thin sections from the drill core are oriented parallel to the length of the core (which is presumed to have intersected the paleohorizontal at a steep angle). The plagioclase grain shape has already been reported for a sub-set of our Skaergaard sample suite by Holness (2015): we re-measured grain shape in these samples for consistency.

It has been argued that the lower half of the Cambridge drill core records the progressive inflation of the Skaergaard chamber (Holness et al., 2015). The lowermost few tens of meters sampled by the drill core are thought to have crystallized from a small sill-like injection of basaltic magma that formed at the contact between the Precambrian gneiss and the overlying sequence of lavas. Well before it crystallized fully, this initial intrusion was inflated by the arrival of successive magma batches to become the Skaergaard magma chamber.

The increase in Mg number at −120 m (**Figure 3**) is not associated with modal banding or grain size reduction but is accompanied by localized polymodal olivine populations (Holness et al., 2015) together with an increase in Θ_{cpp} indicative of decreased super-solidus cooling rates. These observations are consistent with the early inflation of the growing magma chamber by the arrival of at least three relatively small batches of hot, buoyant, olivine-phyric magma that were not chilled sufficiently to result in a high nucleation rate (Holness et al., 2015). We examine three samples from this part of the core.

The decrease in Mg number at −89 m (**Figure 3**), associated with no change in either Θ_{cpp} or grain size, has been argued to indicate the arrival of a small batch of cool, evolved, relatively dense, liquid which ponded on the chamber floor before progressively mixing with the overlying, more primitive bulk magma (Holness et al., 2015). We examined three samples from this part of the core.

The olivine-rich layer at −65 m (**Figure 3**) marks the arrival of a small batch of primitive magma which was quickly and thoroughly mixed with the resident magma (Holness et al., 2015): we examined two samples from this part of the core.

The region of the core between −24 and 40 m records major changes of microstructure, modal mineralogy and trace element composition, indicative of the arrival of a substantial volume of hot and primitive magma and the inflation of the chamber to its final size (Holness et al., 2015). The interval between −2.5 m and about 50 m is marked by a zone of fairly well-defined modal layering that might mark the onset of vigorous convection and mixing in the newly enlarged chamber. The olivine-rich layer at -8.8m is fine-grained (*ibid.*) and may have formed by accumulation from an olivine-phyric magma that rapidly mixed with the resident magma, with little opportunity to develop either a geochemically distinct ponded layer on the chamber floor or a distinct layer of entrained grains of forsterite-rich olivine. We examined two samples from this region of the stratigraphy.

The plagioclase in the Skaergaard samples is highly non-equant (**Figures 4A,B**). Plagioclase-plagioclase grain boundaries in samples with a weak fabric are commonly irregular (**Figure 4A**), whereas those in samples with a stronger fabric are generally smooth, commonly planar, and predominantly parallel to (010) growth faces of one or both grains (**Figure 4B**). Compositional zoning is common: many grains have normally zoned margins whereas some also have highly irregular internal zoning (Maaløe, 1976).

The Rum Eastern Layered Intrusion, Scotland

The Rum Central Complex is part of the British Palaeogene Igneous Province, an area of intense igneous activity formed during continental attenuation prior to opening of the North Atlantic Ocean, and has been dated at 60.53 ± 0.08 Ma (Hamilton et al., 1998). The pre-Palaeogene rocks of Rum mainly comprise a thick succession of Proterozoic (Torridonian) sandstones with the gneissic Archean basement locally exposed within the uplifted parts of the Complex (Emeleus et al., 1996; Emeleus, 1997). Igneous activity on Rum comprised an early, relatively minor, salic stage and a later, wholly mafic to ultramafic stage. The latter forms the Rum Central Complex, which is divisible into the mafic/ultramafic Western, Central and Eastern Layered Intrusions. The contemporaneous Long Loch Fault, running through the center of the island, has been suggested as the prime magma conduit feeding the growing complex (Emeleus et al., 1996).

The Rum Eastern Layered Intrusion was built from numerous replenishments of a shallow sub-volcanic sill-like chamber by variously basaltic (Renner and Palacz, 1987) and picritic (McClurg, 1982; Greenwood et al., 1990; Upton et al., 2002) magma (Emeleus et al., 1996; Holness and Winpenny, 2009). The Eastern Layered Intrusion comprises 16 macro-scale cyclic units comprising a lower peridotite with upper allivalite horizons (a local term describing troctolites or gabbros). This relatively coarse sub-division disguises a great complexity in the modal layering, with the majority of the allivalites containing many subsidiary peridotite horizons (Emeleus et al., 1996; Holness and Winpenny, 2009), ranging in thickness from several meters down to ∼1 cm.

The Unit 10 allivalite is notable for evidence of downward infiltration of picritic magma at the top (Tait, 1984, 1985) and upward infiltration of relatively evolved magma at the base (Holness, 2007; Holness et al., 2012). The bulk geochemistry of a subset of the Unit 10 samples is reported by Tait (1984, 1985). Much of the Unit 10 allivalite is gabbroic, with troctolites confined to the lowest few meters: we chose five samples from the lowest 2 m of the traverse collected by Tait (1984) [denoted Traverse D by Holness et al. (2012)] of which the uppermost is a gabbro. These samples record evidence of

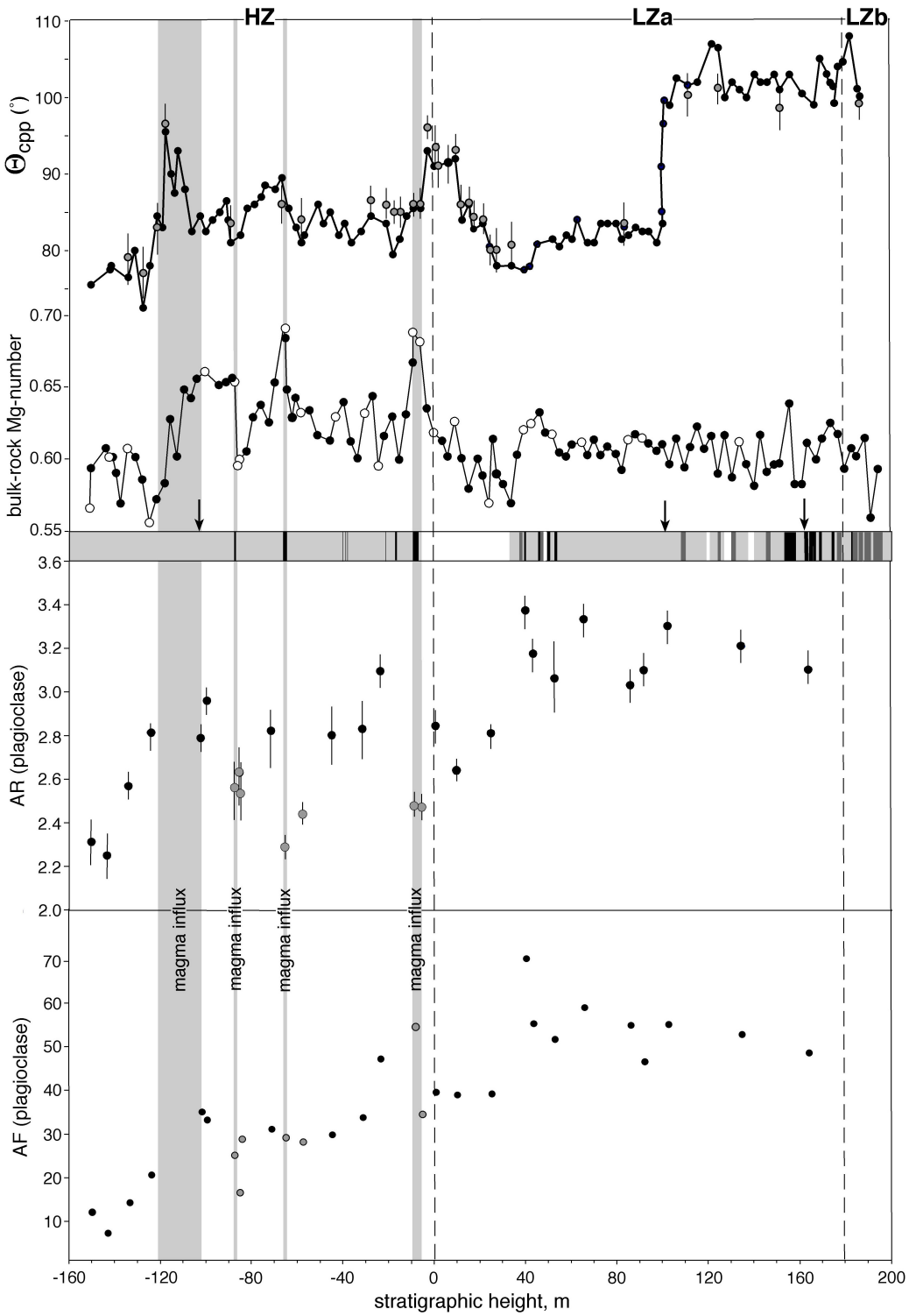

FIGURE 3 | Microstructural and compositional variation through the 1966 Cambridge drill core, sampling the lowest 350 m of the Skaergaard Layered Series. The schematic log shows olivine-rich bands as black, average compositions as gray and leucocratic bands as white [see Holness et al. (2015) for further details]. The stratigraphic variation of clinopyroxene-plagioclase–plagioclase dihedral angle, Θ_{cpp}, and the bulk rock Mg-number are shown [from Holness et al. (2007c, 2015)]. The dotted lines show the divisions into HZ, LZa, and LZb. The vertical gray bands show the regions of stratigraphy identified by Holness et al. (2015) as recording the input of magma into the inflating chamber. Samples described in the present study are shown as open circles in the Mg-number plot if compositional data is available, with the position of the three samples for which no compositional data is available shown as arrows on the schematic log. The variation of plagioclase AF and AR are shown. Those samples denoted by a gray circle are those closely associated with the points marking magma influx and chamber inflation.

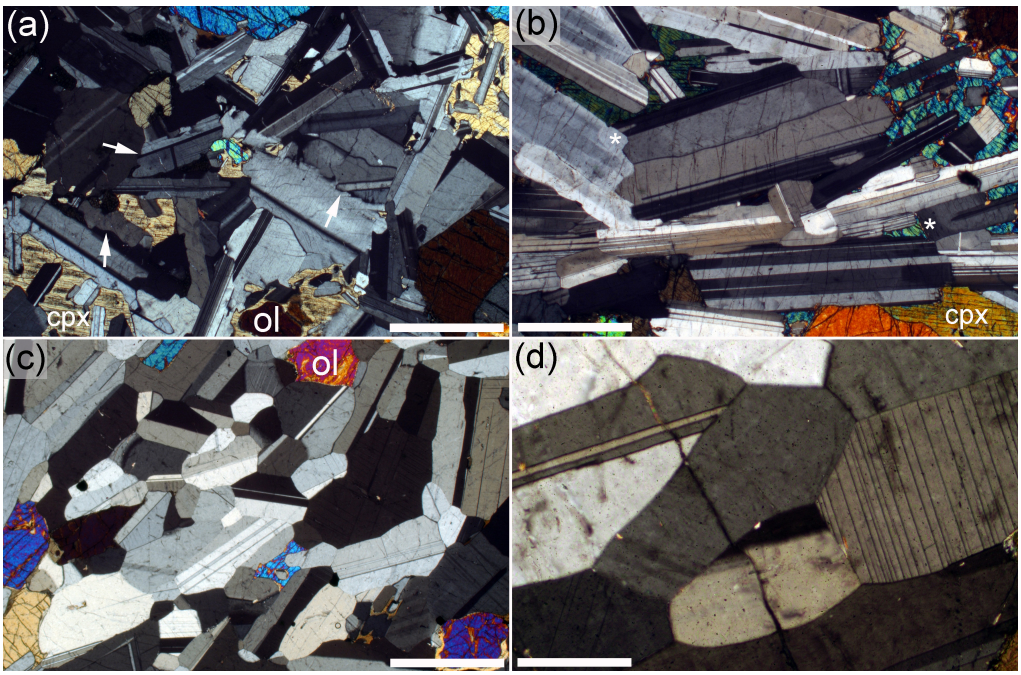

FIGURE 4 | photomicrographs of Skaergaard and Rum troctolites, all photographed under crossed polars. **(a)** Sample from lower part of HZ, containing primocrysts of olivine and plagioclase with interstitial clinopyroxene. There is no preferred alignment of elongate plagioclase. Note the irregularity of the grain boundaries (examples are arrowed) that are not parallel to expected growth faces in the two grains on either side. Scale bar is 1mm long. **(b)** LZa sample from the upper part of the 1966 drill core, in which plagioclase primocrysts show a well-developed shape preferred orientation. Grains are commonly bounded by expected growth faces parallel to (010). Compositional zoning is confined to the ends of the elongate laths (examples are shown by asterisks), demonstrating that grain boundaries parallel to the large (010) faces were formed as equant grains were brought together mechanically. Scale bar is 1 mm long. **(c)** Troctolite from Unit 12 of the Rum Eastern Layered Series. Note the rounded grain boundaries in the plagioclase-rich regions, with significant modification of the original euhedral shape of these primocrysts. Scale bar is 1mm long. **(d)** Plagioclase-rich region of Rum Unit 12 troctolite demonstrating the almost granular microstructure indicative of extensive sub-solidus textural equilibration. Scale bar is 200 μm long.

significant, post-accumulation, upward infiltration of evolved magma derived from the underlying peridotite.

The Unit 12 allivalite is predominantly troctolitic with several subsidiary peridotite horizons interpreted as the record of replenishment events (Holness and Winpenny, 2009). No bulk rock geochemical data are available for the Unit 12 samples, although mineral compositions are reported by Holness and Winpenny (2009). We chose four samples of Unit 12 troctolitic cumulates, located sufficiently far from the subsidiary peridotites that they are unlikely to have been affected by changes in cooling rate due to the presence of nearby hot picritic magma (Holness and Winpenny, 2009). Sections were cut perpendicular to any fabrics.

The Rum troctolites are dominated by olivine and plagioclase, with several of our samples close to perfectly adcumulate (**Table 2**). Minor quantities of interstitial clinopyroxene are present, commonly forming thin rims separating olivine and plagioclase primocrysts, although clinopyroxene forms oikocrysts in several of the Unit 10 troctolites. The median clinopyroxene-plagioclase-plagioclase dihedral angle, Θ_{cpp}, in the Rum troctolites unaffected by late-stage infiltration is 80–85° (Holness, 2007; Holness and Winpenny, 2009). Cr-spinel may be present in small quantities (<2 vol.%). Evolved phases such as apatite, low-Ca pyroxene and Fe-Ti oxides are absent. The plagioclase in the Rum troctolites is slightly elongate (as viewed in thin section) and is characterized by smooth plagioclase-plagioclase grain boundaries (**Figure 4C**), with a granular microstructure (i.e., almost equant grains) developed in relatively finer-grained plagioclase-only regions (**Figure 4D**). In comparison with the Skaergaard troctolites, very few grain boundaries are planar and parallel to the (010) faces of the adjacent grains. There is no evidence of plastic deformation by dislocation creep. Weak intra-crystalline plagioclase compositional zoning is locally present.

MATERIALS AND METHODS

Plagioclase apparent aspect ratio in natural samples was measured using either photomicrographs or a high-quality scan of entire thin sections under crossed polars. Thin sections were oriented perpendicular to any foliation where visible, and parallel to the drill core (and hence, to the best of our knowledge, perpendicular to the paleo-horizontal). The long and short axis of each grain intersection were drawn on by hand and the aspect ratio was calculated using the Feret diameter tool of ImageJ. Previous work on the shapes and orientations of plagioclase enclosed in pyroxene oikocrysts has demonstrated that there are

TABLE 2 | Details of samples from the Rum Eastern Layered Intrusion.

Sample	Height (m)	Mineral modes (vol.%)				AR	AR Min	AR Max	Plag length (mm)	AF	*n*
		Plag	Ol	Augite	Cr-spinel						
Unit 10											
146196	0.1	69.2	27.8	1.5	1.5	2.23	2.18	2.27	0.668	20.77	351
146197	0.4	60.1	21.9	18.0	0.0	2.32	2.28	2.36	0.732	35.72	403
146198	0.6	68.1	14.5	16.9	0.5	2.62	2.58	2.69	0.719	56.79	280
146199	0.7	57.6	34.9	7.5	0.0	2.44	2.39	2.49	0.822	44.16	267
146200	1.9	56.5	11.4	32.1	0.0	2.37	2.32	2.41	0.914	32.04	275
Unit 12											
R12-J7	6.40	72.5	23.5	1.5	2.5	2.10	2.06	2.14	0.873	47.00	322
R12-J13	11.40	74.0	18.1	5.5	2.4	2.27	2.23	2.31	1.015	56.53	293
R12-J16	14.27	75.8	19.6	1.3	3.3	2.36	2.31	2.40	1.084	59.92	259
R12-J30	7.95	72.9	25.2	1.5	0.4	2.18	2.15	2.21	0.867	56.81	289

*Abbreviations as for **Table 1**.*

commonly systematic differences between enclosed plagioclase and that outside oikocrysts, with the enclosed grains thought to preserve the early structure of the mush (**Figure 1B**; Mathison, 1987; Higgins, 1991, 1998). Some of our samples contain a few grains of poikilitic pyroxene, and for consistency, we avoided analyzing plagioclase grains enclosed in oikocrysts: every other visible plagioclase grain was analyzed in each image or scan. Between 171 and 451 grains were measured for each sample. The 2σ confidence interval on the average aspect ratio was constrained using bootstrap sampling: a method suitable for populations of measurements for which the shape of the underlying distribution is unknown. Results are reported in **Tables 1**, 2.

Our values of AR for the sub-set of Skaergaard samples measured by Holness (2015) are consistently lower than previously reported: we suggest this is because we used higher resolution images for the present study, permitting the inclusion of the complete grain population in each thin section. The alignment factor, AF, was calculated according to the method of Meurer and Boudreau (1998), by which a value of 100 denotes perfect alignment to form a foliation and one of 0 denotes perfectly random orientation.

Plagioclase–plagioclase–plagioclase dihedral angles were measured using a 4-axis Leitz universal stage mounted on a James Swift monocular microscope fitted with a 32× long working distance objective. 33 randomly chosen individual three-grain junctions were measured for each sample, resulting in a population of 99 dihedral angles (though note that only 2/3 of this population represents independent values). We report the standard deviation of this population.

The apparent aspect ratio of 3D cuboid grains cut by randomly oriented planes was calculated according to the method of Morgan and Jerram (2006), using two endmembers. The first assumes a completely random orientation of crystals of a given shape and size, whereas the other assumes a perfect foliation. For comparison with the natural samples, we calculated the shape and cross-sectional area of 2,000 grain intersections for the two endmembers for the seven different grain shapes 1:1.5:2, 1:2:3, 1:2:4, 1:2:6, 1:3:7, 1:4:7, and 1:5:8, when viewed perpendicular to foliation. The aspect ratio of each grain intersection was calculated using the fit ellipse function of ImageJ. Note that in creating these synthetic populations, no allowance was made for space-filling constraints which prevent crystals attaining these idealized cuboids when forming a poly-crystalline aggregate.

RESULTS

Skaergaard and Rum Grain Shapes and Fabrics

There is a well-defined increase in plagioclase alignment factor (AF) with increasing stratigraphic height in the lower part of the Skaergaard stratigraphy, with a region of approximately constant AF between −100 and 0 m stratigraphic height, followed by an increase to higher, but rather scattered, values at 40 m stratigraphic height (**Figure 3**). AR also broadly increases with stratigraphic height (**Figure 3**), but with a sharp increase in the lower part of the stratigraphy, a region of broadly constant AR between −100 and 20 m height, and then a region of higher but variable AR in the upper part of the core. Notably, locally low values of AR are closely associated with three of the episodes of magma influx identified by Holness et al. (2015) (at −89, −65, and −8 m). We identified seven samples with anomalously low values of AR (shown as gray symbols in **Figure 3**). Three of these seven samples contain finer-grained plagioclase than the rest of the suite (**Table 1**).

The microstructural data from the main group of samples form a positive correlation on a plot of AF against AR (the Skaergaard main trend), while the seven samples with lower than expected AR form an almost AR-invariant group, albeit with a lot of scatter (the Skaergaard second trend) (**Figure 5**). Extrapolation of the best-fit line through the data points forming the main trend gives an AR of 2.10 for fully random samples (AF = 0) and 4.05 for perfectly foliated samples (AF = 100).

The Rum samples from the two allivalite units form two clearly distinct groups on a plot of AR against AF (**Figure 5**), each with a positive slope, but offset to lower AR than the Skaergaard main trend. The single gabbroic sample from Unit 10 is indistinguishable from the Unit 10 troctolites on this plot.

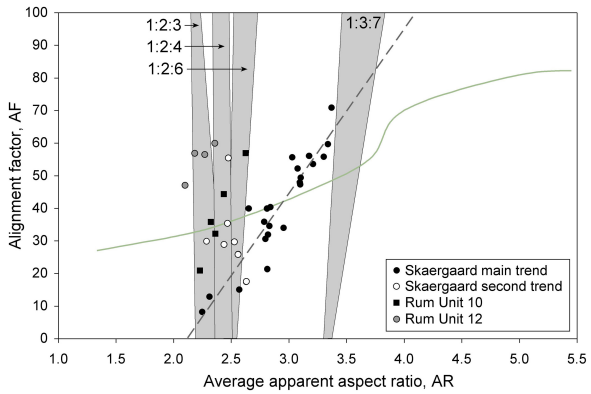

FIGURE 5 | The variation of alignment factor (AF) as a function of average apparent aspect ratio (AR) for the Skaergaard and Rum troctolites. The continuous green line shows the trend reported by Meurer and Boudreau (1998) for Stillwater cumulates. The shaded boxes show the range of correlations expected for rocks containing grains of a constant (cuboid) shape (see labels). The left-side of each box is that calculated without the 5% smallest grain intersections, and the right-side of the box is that calculated without the 20% smallest grain intersections. In all cases, the calculated trend for the synthetic systems with constant grain shape is steeper than that observed for the natural samples, suggesting that the trend in the natural samples is caused at least in part by less equant grains in samples with stronger fabrics. The dashed line shows the best fit through the main group of Skaergaard samples.

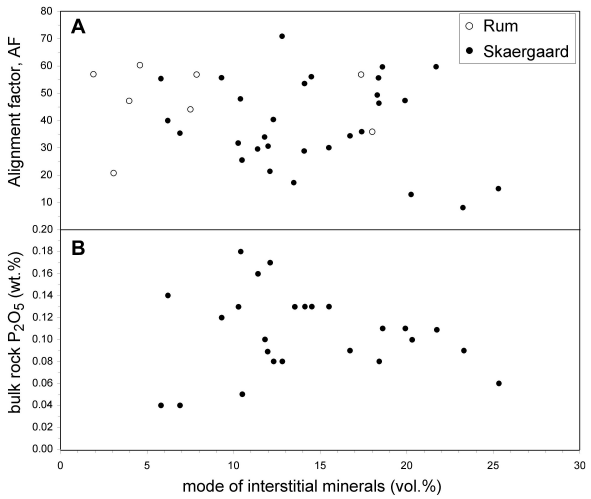

FIGURE 6 | (A) The variation of alignment factor (AF) as a function of the volumetric proportion of interstitial phases (i.e., all phases other than plagioclase and olivine) in the Skaergaard and Rum troctolites. **(B)** The variation of bulk rock P_2O_5 [reported by Holness et al. (2015) and shown in **Table 1**] as a function of the volumetric proportion of interstitial phases in the Skaergaard troctolites.

In agreement with McBirney and Hunter (1995), we find no correlation between the volumetric proportion of interstitial minerals and fabric strength (**Figure 6A**) in either the Rum or the Skaergaard troctolites. Similarly, there is no correlation between the amount of interstitial minerals and the bulk rock P_2O_5 concentration in the Skaergaard troctolites (**Figure 6B**).

Apparent Grain Shapes and Fabrics in Synthetic Systems

A population of randomly chosen grain intersections through isolated perfect cuboids includes many very small slices, commonly with high aspect ratio (Higgins, 1994). Such small slices are not observed in natural samples of plutonic rocks, because of the constraints placed on grain shape by the necessity of space-filling. Additionally, one might expect that the overall grain size of the natural samples would control the observed population of grain intersections, with the chance of observing a slice with an extreme aspect ratio increasing with increasing overall grain size. However, this effect will be modified by the effects of the overall thickness of the thin section, which makes detecting slices cut <30 μm from the grain edge difficult. The problems associated with the absence of detailed modeling either of the way the effective cut-off changes with grain size, or of the effect of space-filling constraints on the shape corners and edges of crystals in fully solidified rocks, are minimized if the 2D grain shape is parameterized by the mode of the population of apparent aspect ratios (e.g., Higgins, 1994). However, to permit direct comparison with previous studies of the plagioclase grain shape in natural examples (Meurer and Boudreau, 1998; Holness, 2014), we chose to use the average apparent aspect ratio.

To permit comparison of our populations of intersections of isolated cuboids with the cumulates, we calculated the way the average aspect ratio of the synthetic population changes with progressive exclusion of the smallest grain intersections (quantified by area) (**Figure 7**). For all cuboid shapes, once the smallest ∼50 grain intersections are ignored the average apparent aspect ratio in the perfectly foliated population is higher than that in the population with randomly oriented cuboids (**Figure 7**). The difference between AR in the perfectly foliated and that in the population with random cuboid orientation generally increases with greater exclusion of the smaller intersections. We do not consider, however, the populations involving only the few hundred largest intersections (i.e., those parts of the curves toward the right in **Figure 7**) to be comparable to the natural samples.

The average apparent aspect ratios for the cuboid shapes 1:4:7 and 1:5:8 lie entirely outside the range 2.25–3.37 (i.e., that range observed for the Skaergaard main trend, **Table 1**), while that for 1:1.5:2 lies in that range only if almost all the small interactions are included (**Figure 7**). These three shapes are therefore unlikely to be similar to those found in the Skaergaard cumulates forming the main trend on the plot of AR vs. AF.

For the shapes 1:2:3, 1:2:4, and 1:2:6, the average apparent aspect ratio of populations containing all but the smallest 5% of the intersections and of populations containing all but the smallest 20% intersections (i.e., those populations likely to most closely approximate natural samples), fall in the range 2.25–3.37. Intersections of cuboids with the shape 1:3:7 have a generally higher aspect ratio than observed in the Skaergaard samples,

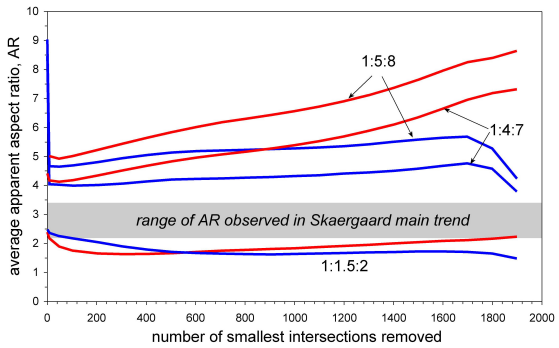

FIGURE 7 | The variation of average apparent aspect ratio (AR) for synthetic rocks comprising grains of constant shape (either 1:1.5:2, 1:4:7, or 1:5:8) as a function of the completeness of the population of grain intersections. The shape of a total of 2,000 intersections was calculated, and AR was calculated by omitting progressively more of the smallest intersections. For each of the three shapes, the red line shows the variation of AR in a perfectly foliated system while the blue line shows that for entirely randomly oriented grains. The horizontal gray box shows the range of AR found in the main group of Skaergaard troctolites (shown in **Figure 5**).

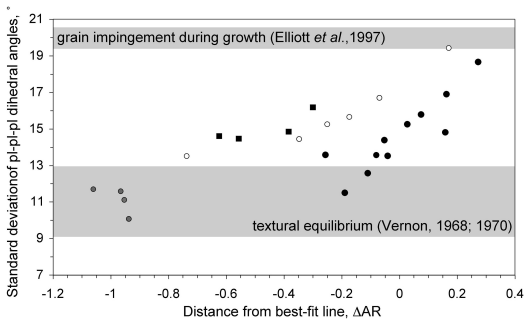

FIGURE 8 | The standard deviation of populations of plagioclase–plagioclase–plagioclase dihedral angles in the Skaergaard and Rum troctolites as a function of the difference, ΔAR, between the observed AR and the expected AR were the sample to fall on the line of best fit through the main group of Skaergaard data (shown in **Figure 5**). Symbols as in **Figure 5**. The horizontal gray boxes show the reported values of standard deviation for fully texturally equilibrated samples (from Vernon, 1968, 1970) and that consistent with random impingement of growing grains (from Elliott et al., 1997).

but fall into the range if they are randomly oriented. The range of likely average apparent aspect ratios in rocks containing plagioclase grains with these four shapes is shown in **Figure 5**. As the grain shape becomes increasingly less equant, the difference in AR between the random and the foliated microstructures increases, but in none of the four cases does it increase as much as is observed for the Skaergaard main trend and the two suites of Rum samples (**Figure 5**).

The Extent of Sub-Solidus Textural Equilibration

The standard deviation of plagioclase–plagioclase–plagioclase dihedral angle populations in a selection of samples from Skaergaard and Rum is shown in **Figure 8**. Since progressive textural equilibration is expected to change grain shape without having much effect on crystallographic orientation, we plotted standard deviation of the dihedral angles as a function of the difference between the actual observed AR and the expected AR were the sample to fall precisely on the best-fit line through the main grouping of Skaergaard data. Thus, a positive ΔAR is calculated for samples falling on the right of the dashed line in **Figure 5**, and a negative ΔAR is calculated for those falling on the left.

The data fall into three well-defined groups. The analyzed subset of the main Skaergaard trend (comprising samples covering the full range of observed ΔAR) shows a steeply decreasing standard deviation, from values close to those expected for impingement (Elliott et al., 1997) to those expected for textural equilibrium (Vernon, 1968, 1970), as ΔAR decreases. The Skaergaard second group (represented by six of the seven samples) also show this correlation, but with a shallower slope and offset to more negative values of ΔAR; the Rum Unit 10 samples fall very close to this group. The final group comprises the Rum Unit 12 samples, which form a tight cluster with standard deviations indicative of textural equilibrium.

DISCUSSION

Comparison With Previous Work

Our observations demonstrate a greater sensitivity of the strength of fabrics to plagioclase grain shape in troctolites than that originally proposed by Meurer and Boudreau (1998) for cumulates from Stillwater (**Figure 5**). It is unlikely that this difference is a consequence of different plagioclase modes in the two sets of samples, since the Meurer and Boudreau (1998) samples all appear to have a similar range of mineral modes to that in the cumulates analyzed here. A major difference between our study of the Rum and Skaergaard cumulates and Meurer and Boudreau's (1998) work on Stillwater is that the latter did not include all plagioclase grains in their measurement populations, whereas we measured all those grains which were visible in each photomicrograph.

The relationship between AR and AF found by Meurer and Boudreau (1998) (**Figure 5**) is that expected for samples that have undergone significant textural equilibration, since it can be extrapolated to finite values of AF for fully equant grains (**Figure 2**). It would be instructive to re-examine their samples and measure the standard deviation of plagioclase–plagioclase–plagioclase dihedral angles to determine how closely they have approached textural equilibrium.

Grain Shape and Fabric Strength

A comparison of the variation in the calculated average apparent aspect ratio as a function of fabric strength in the synthetic rocks and in the samples from Rum and the Skaergaard main trend demonstrates that the positive correlation between AR and AF observed in the natural samples is highly unlikely to

be an artifact created by the fabric itself. Instead, a comparison of the data derived from the synthetic systems suggest that the observed increase in AR with increasing alignment factor in the main group of Skaergaard samples is associated with a change in general grain shape from something in the range 1:2:3–1:2:6 to 1:3:7 (**Figure 5**). It should be remembered, however, that it is unlikely that the natural samples contain only a single grain shape and that the observed trend is most probably a result of the entire range of shapes becoming less equant.

That the strongest fabrics (highest AF) correlate with high AR is due to some combination of fabric creation being easier for more elongate plagioclase grains in either flowing magma or in a mush undergoing seismic activity (i.e., AR is the controlling factor), and the limitations on growth caused by the impingement of (010) faces (i.e., AF is the controlling factor). Working out which of these two processes is dominant is not straightforward.

The strong correlation between position relative to the best fit line on the AR vs. AF plot (**Figure 5**) and the extent of textural equilibration of the plagioclase–plagioclase–plagioclase three-grain junctions (**Figure 8**), suggests that the scatter of both the main and the second group of Skaergaard samples, and the cumulates from Rum Unit 10 from their respective lines of best fit, is at least partly a consequence of variable extents of textural equilibration: those samples in which sub-solidus cooling rates were sufficiently slow to permit the completion of the first stage of textural equilibration (and therefore a low standard deviation) have a relatively low AR. Such sub-solidus reduction in average aspect ratio of the original grains grown during solidification is likely to be most pronounced for the smaller plagioclase grains in the sample, although we do not have sufficient grains in our thin sections to test this hypothesis.

Figure 8 also demonstrates that the lower AR found in the second group of Skaergaard samples and the Rum Unit 10 cumulates cannot be a result of a comparatively close approach to textural equilibrium, since the standard deviation of dihedral angles at plagioclase triple junctions in these samples is too high. Instead, the original plagioclase grains in these samples must have been more equant than those in the main Skaergaard group, perhaps with shapes in the range 1:2:3–1:2:6 (**Figure 5**). The different shape probably accounts for the more shallow slope for these samples in **Figure 8**: the choice of abscissa in **Figure 8** is only meaningful for the Skaergaard main group of data.

The troctolites in the Rum Unit 12 have a similar range of alignment factor as those from Unit 10, but lower aspect ratio (**Figure 3**). This lower aspect ratio is associated with plagioclase three-grain junction geometry that appears to be in, or very close to, textural equilibrium (**Figure 8**). The complete Rum data set forms a well-defined positive correlation on the plot of standard deviation vs. ΔAR (**Figure 8**), suggestive of a grain shape in Unit 12 originally indistinguishable from that in Unit 10 but with significant modification during sub-solidus textural equilibration (c.f. Vernon, 1970), consistent with slower sub-solidus cooling of the floor during and immediately after the formation of Unit 12. The Unit 12 allivalite records seven replenishment events after the arrival of the magma that forms the base of the allivalite (Holness and Winpenny, 2009) and we suggest that this continuous replenishment of the open-system magma chamber prevented significant cooling of the recently solidified cumulates, leading to extensive sub-solidus textural equilibration.

Changes in Fabric Strength Through the Lower Part of the Skaergaard Stratigraphy

The well-defined general increase in fabric strength with increasing stratigraphic height in the Skaergaard Layered Series troctolites (**Figure 3**) is associated not only with an increasingly non-equant plagioclase grain shape but also with a progression from microstructures indicative of *in situ* nucleation and growth (**Figures 1A**, **4A**) to those expected for mushes in which accumulated crystals have been re-arranged by magmatic currents (**Figures 1B**, **4B**). We suggest that these changes record the early inflation of the Skaergaard chamber and the changing location of crystallization as cooling proceeded subsequent to full inflation.

The formation of a horizontal tabular intrusion splits the geotherm, ensuring that cooling is fastest at the roof (Morse, 1986), leading to convection [both thermal and two-phase (e.g., Grout, 1918)]. Because the change in temperature of the liquidus and adiabat with increasing pressure are different, down-welling magma in an intrusion of km-scale height becomes super-cooled, driving nucleation and crystal growth in the down-welling plumes and ensuring that crystallization occurs near the chamber floor (Irvine, 1970). The resulting predominance of crystallization near the floor, amplified by the accumulation of crystals nucleated at the roof and walls and brought down by convection currents, means that crystal accumulation is greatest on the floor of the magma chamber, with the stratigraphic position of the most evolved floor cumulates closer to the roof than the base of the stratigraphy. This asymmetry of crystal accumulation amplifies the asymmetry of cooling by creating an insulating blanket of mush on the floor, made more effective by the release of latent heat during the solidification of interstitial liquid. The insulating floor blanket prevents the large undercooling required for *in situ* nucleation of crystals from the bulk magma (i.e., primocrysts) at the floor itself. Morse (1988) suggests that ∼100 m of floor blanket is required to make a discernible difference to the location of crystal nucleation and growth from the bulk magma. Thus it is only possible to nucleate primocrysts directly on the chamber floor in an intrusion of km-scale height immediately after magma emplacement, with crystals supplied to the floor during the later stages of solidification by migration of those nucleated at the roof and walls. Microstructures in the floor cumulates are thus dominated by those indicative of *in situ* nucleation and growth only in the lowermost parts of the stratigraphy, being replaced by those indicative of crystal transport and re-arrangement by magmatic currents higher in the stratigraphy.

Note, however, that this scenario applies only to bodies created by a single magma batch, or by a series of batches that are sufficiently closely spaced in time to be treated as effectively one single batch. The location of crystal nucleation and growth in open systems replenished by batches of super-heated magma will be different (e.g., Latypov et al., 2017).

The Skaergaard chamber filled progressively, likely beginning as a sill, with full inflation marked by the arrival of a major magma injection once ∼150 m of the stratigraphy had formed. The microstructural evidence points to a transient initial period of *in situ* nucleation on the chamber floor, both because the chamber in its earliest stages was a thin sill, and because the thermal blanket on the floor had not developed, allowing enough heat loss through the floor to create sufficient undercooling to permit nucleation on the floor itself. As the chamber inflated, the increased height promoted convection both because cooling through the roof dominated over that at the floor, and because of an increased contribution to cooling at the increasingly extensive vertical walls. The onset of convection would lead not only to a substantial increase in the amount of material brought to the chamber floor, a decrease of *in situ* heterogeneous nucleation on the chamber floor itself, and also to the creation of fabrics as the convection currents aligned the accumulated grains, evident as increasingly well-developed SPO fabrics upward in the Skaergaard stratigraphy.

We suggest that the stratigraphic variation of AF observed in the lower 320m of the Skaergaard stratigraphy (**Figure 3**) is consistent with the conclusions of Holness et al. (2015): a rapid inflation of an initial sill-like body is recorded in the core between −120 and −100 m depth, followed by a period in which the chamber inflated only by a small amount following injections of magma at −89 and −65 m. The chamber attained its final height with the major injection recorded in the drill core at −8 m. The two events which significantly changed the height of the chamber are associated with step-wise increases in AF. We suggest these increases are due to step-wise increases in convective strength, due to the greater influence of cooling at the increasingly important vertical walls and the greater asymmetry of cooling at the roof and floor.

Note that Campbell (1978), following an assessment of the various ways in which adcumulates may form, argues for *in situ* heterogeneous nucleation throughout the development of floor cumulates, with only minimal contribution to the floor mush of crystals nucleated and grown elsewhere in the chamber. However, the concentration of clear microstructural evidence for *in situ* nucleation and growth only in the lowest part of the stratigraphy suggests that this was not the case in the Skaergaard. Above the first few tens of meters of stratigraphy, the crystal pile on the chamber floor grew by the accumulation of significant quantities of crystals either sourced elsewhere, nucleated just above the magma-mush interface in downwelling plumes (e.g., Morse, 1986), or formed in a floor mush that could be easily disaggregated to form secondary fabrics.

While the above explanation can account for the observed stratigraphic variation in fabric strength and the extent of microstructural evidence for *in situ* grain growth, we have not yet discussed the associated changes in grain shape. Although we cannot yet unambiguously differentiate which of the two primary drivers for the positive correlation between AR and AF is dominant, we ought to consider what might be causing an upward increase in AR in the absence of any effects of increasing AF.

The aspect ratio of non-equant minerals undergoing *in situ* growth is affected by the timing of impingement against adjacent grains, with early impingement resulting in a lower aspect ratio (Martin et al., 1987). Thus, the marked increase in AR observed in the lowermost 40m of the stratigraphy (**Figure 3**) could be a consequence of a decreasing significance of *in situ* nucleation and growth as the insulating floor blanket developed. An increase in plagioclase aspect ratio can also be achieved by an increase in the cooling rate (Holness, 2014). However, the rate of cooling through the floor, and the overall rate of heat loss from the intrusion, decrease with time. A cooling-rate-controlled increase in AR can therefore only be recorded in the floor cumulates if they have an increasing component of accumulated crystals sourced from rapidly cooling parts of the chamber such as the roof and walls.

During the earliest history of the Skaergaard intrusion, the wall mush was relatively strong, with only localized evidence for tearing and disruption caused by collapse. As solidification proceeded, the mush developed diffuse patches of coarse-grained, relatively evolved material interpreted to have formed during the collapse and tearing of a progressively weaker and more poorly consolidated mush (Humphreys and Holness, 2010). This decreasing coherence would have been associated with an increase in the amount of crystals lost from the inner margin of the mush and therefore an increase in the rate of supply of sediment to the floor. Since the plagioclase formed at the rapidly cooling wall is likely to be less equant than that grown at the more slowly cooled floor, an increase in the contribution of the wall mush to the floor cumulates would be recorded in an increase in AR upward through the stratigraphy.

Localized Departures From the Main Skaergaard Trend

Three of the four regions of the stratigraphy associated with evidence for magma influx are marked by relatively equant plagioclase (**Figure 3**), with a narrow range of AR, despite a wide range of alignment factor (**Figure 5**). Two of these three replenishment events, those at −65 and −8 m, involved the arrival of hot primitive magma (Holness et al., 2015). The cumulates at these points in the stratigraphy are relatively fine-grained and have low AR compared to nearby samples (**Table 1** and **Figure 3**). The fine grain size is likely to be a consequence of chilling of the incoming magma, leading to a high nucleation rate. The relatively low AR may be a consequence of early impingement (consequent to the high nucleation rate) or because the growth rate of the plagioclase slowed on the arrival of hotter magma. That cooling rate may have been a dominant influence on plagioclase shape is suggested by the observation that AF is not unusually low in these samples, indicating no significant increase of *in situ* nucleation and growth on the chamber floor.

The arrival of magma recorded at −89 m stratigraphic height is associated with a reduction of Mg#, denoting evolved cool magma (**Figure 3**; Holness et al., 2015). The associated reduction in AR is not particularly marked (**Figure 3**) and there is no change in the grain size (**Table 1**). We suggest that the relatively small decrease in AR (compared to the influxes at −65 and −8 m) was

a result of an increase in the contribution of *in situ* nucleation to the growth of the floor mush as the temperature of the magma chamber decreased, consistent with the single sample from this region of the core with weak fabric.

The prolonged magma injection event recorded between about −120 and −100 m depth in the core, which increased the chamber height sufficiently to create a step-wise increase in convective strength (recorded in an increase in AF) is not associated with lower than expected values of AR (**Figure 3**). We suggest that the relatively long duration of this event, involving at least three batches of magma (Holness et al., 2015), did not result in discrete chilling events that could be detected on the length scale of our sampling. We suggest that a closer sampling strategy through this part of the core might pick up localized excursions in grain size and shape.

Comparison of Rum and Skaergaard Troctolites

The main fabric-forming mechanisms in the Rum and Skaergaard chambers are likely to have been different. There is no evidence of vertical walls in the generally tabular Rum chamber, and none of the roof is preserved *in situ*. However, abundant evidence of slumping attests to frequent tectonic disturbance (O'Driscoll et al., 2007) and we suggest that the fabrics in the Rum troctolites are due to the disaggregation and re-arrangement of the mush by external tectonic events (e.g., Davis et al., 2007), rather than the strong convection currents active in the Skaergaard chamber [i.e., that the Rum fabrics are secondary, rather than primary, according to the classification scheme of Holness et al. (2017)].

The values of Θ_{cpp} in the troctolites of the Rum Eastern Layered Intrusion that are not affected by late-stage infiltration are similar to those reported for troctolites in the Skaergaard intrusion (Holness, 2015), consistent with similar solidification rates of the floor mush in the two intrusions. That the original grain shape of plagioclase in the Rum troctolites is generally more equant than that seen in most of the Skaergaard samples (**Figure 3**), suggests that growth rates of plagioclase at the roof of the open-system, continually replenished, sill-like Rum chamber was slower than at the roof and walls of the closed-system Skaergaard chamber.

The Effect of Fabric on Mush Structure and Adcumulus Status

Following Wager (1963), the most commonly used parameter to determine adcumulus status is the bulk rock concentration of incompatible elements such as P_2O_5. Accordingly, there should be a correlation between the bulk rock concentration of highly incompatible elements and the mode of minerals grown from the interstitial liquid, but this is not generally observed (McBirney and Hunter, 1995; Meurer and Meurer, 2006; Karykowski and Maier, 2017). As pointed out by McBirney and Hunter (1995), and verified here, there is no such correlation between bulk rock P_2O_5 and the mode of interstitial minerals in the Skaergaard troctolites (**Figure 6B**), due perhaps to the progressive loss or addition of interstitial liquids during solidification (Karykowski and Maier, 2017), or to difficulties in nucleating apatite which ends up crystallizing in channels through which late-stage liquids flowed (Meurer and Meurer, 2006). Thus, bulk rock P_2O_5 concentrations are unlikely to be a good measure of the extent to which cumulates contain late-stage liquids.

Although one might perhaps expect adcumulate rocks to develop from a mush in which the accumulated crystals were efficiently packed with a low initial porosity, we found no correlation between the strength of foliation and the mode of interstitial minerals for either the Rum or Skaergaard troctolites (**Figure 6A**). This is in agreement with the findings of McBirney and Hunter (1995), and also with Wager (1963) who stated that "the effect on the phosphorus content of variation in the initial packing is considered slight, compared with the effects of adcumulus growth." Thus the development of adcumulates requires processes other than efficiently packed grains in a strongly foliated rock.

CONCLUSION

The strength of foliations defined by shape preferred orientation of plagioclase in troctolitic cumulates from both the Rum Eastern Layered Intrusion and the Skaergaard intrusion increases as the grains become more tabular, due either to the greater propensity of highly non-equant grains to be re-arranged by magmatic currents or tectonic disruption of poorly consolidated mush, or by the effects of a pre-existing fabric on final grain shape in fully solidified rocks. The stratigraphic evolution of grain shape, microstructures and fabrics in the lower part of the Skaergaard Layered Series records the progressive inflation of the chamber to its final size. Our microstructural observations are consistent with a decrease in the extent of *in situ* nucleation and growth on the chamber floor as the gradually thickening crystal pile created an insulating blanket and to an increasing contribution of both convection and the accumulation of crystals derived from the walls of the expanding magma chamber, as predicted by Irvine (1970) and Morse (1988). That the overall plagioclase grain shape becomes more equant at higher levels in the stratigraphy than those examined here (Holness, 2015) is likely to be primarily a consequence of decreasing cooling rates. The convective strength would likely remain high for most of the remaining stratigraphy, until crystallization had proceeded sufficiently to decrease the height of the remaining magma and as the country rocks heated up appreciably.

Igneous microstructures can be modified during slow sub-solidus cooling: although alignment factor is likely to remain constant (leading eventually to a CPO in a granular rock), textural equilibration leads to a decrease in grain aspect ratio and an approach to equilibrium geometry of three-grain junctions. This is clearly evident in the Unit 12 troctolites of the open-system magma chamber of the Rum Eastern Layered Intrusion. The observation that the standard deviation of plagioclase–plagioclase–plagioclase dihedral angles varies in a systematic manner with the average grain shape suggests that this might

be a useful new parameter to quantify the thermal history of cumulates. More work should be done to explore this variation.

DATA AVAILABILITY STATEMENT

The datasets generated for this study are available on request to the corresponding author.

AUTHOR CONTRIBUTIONS

MH wrote the manuscript and collected some of the data. CM and ZV collected some of the data. DM did the numerical analysis of grain intersections in synthetic systems. All authors contributed to the article and approved the submitted version.

FUNDING

This work was supported by a grant from the Natural Environment Research Council (grant number NE/N009894/1). ZV was supported by a Marie Skłodowska-Curie Fellowship (grant number 708131-EFOX). CM was supported by the Robert Wright Fund of Trinity College, Cambridge, and the John Muir Foundation.

ACKNOWLEDGMENTS

We are grateful to Eric Ferre and Tony Morse for helpful and insightful reviews, and to Michael Higgins and Rais Latypov for their helpful comments on an early version of the manuscript. All remaining misconceptions are our own.

REFERENCES

Arvidson, R. S., Beig, M. S., and Luttge, A. (2004). Single-crystal plagioclase feldspar dissolution rates measured by vertical scanning interferometry. *Am. Mineral.* 89, 51–56. doi: 10.2138/am-2004-0107

Bergantz, G. W., Schleicher, J. M., and Burgisser, A. (2017). On the kinematics and dynamics of crystal-rich systems. *J. Geophys. Res. Solid Earth* 122, 6131–6159. doi: 10.1002/2017jb014218

Boorman, S., Boudreau, A., and Kruger, F. J. (2004). The lower zone – critical zone transition of the bushveld complex: a quantitative textural study. *J. Petrol.* 45, 1209–1235. doi: 10.1093/petrology/egh011

Boudreau, A. E., and McBirney, A. R. (1997). The Skaergaard Layered Series. Part III. Non-dynamic layering. *J. Petrol.* 38, 1003–1020. doi: 10.1093/petroj/38.8.1003

Brothers, R. N. (1964). Petrofabric analyses of Rhum and Skaergaard layered rocks. *J. Petrol.* 5, 255–274. doi: 10.1093/petrology/5.2.255

Brown, G. M. (1956). The layered ultrabasic rocks of rhum, inner hebrides. *Philos. Trans. R. Soc. Lond. Ser. B* 240, 1–53. doi: 10.1098/rstb.1956.0011

Campbell, I. H. (1978). Some problems with the cumulus theory. *Lithos* 11, 311–321.

Campbell, I. H., Roeder, P. L., and Dixon, J. M. (1978). Plagioclase buoyancy in basaltic liquids as determined with a centrifuge furnace. *Contrib. Mineral. Petrol.* 67, 369–377. doi: 10.1007/bf00383297

Davies, I. C., and Walker, R. G. (1974). Transport and deposition of re-sedimented conglomerates: the Cap Enrage formation, Cambro-Ordovician, Gaspe, Quebec. *Sediment. Res.* 44, 1200–1216.

Davis, M., Koenders, M. A., and Petford, N. (2007). Vibro-agitation of chambered magma. *J. Volcanol. Geothermal Res.* 167, 24–36. doi: 10.1016/j.jvolgeores.2007.07.012

Denison, C., Carlson, W. D., and Ketcham, R. A. (1997). Three-dimensional quantitative textural analysis of metamorphic rocks using high-resolution computed X-ray tomography: part I. *Methods Tech. J. Metamorphic Geol.* 15, 29–44. doi: 10.1111/j.1525-1314.1997.00006.x

Donaldson, C. H. (1974). Olivine crystal types in harrisitic rocks of the Rhum pluton and in Archean spinifex rocks. *Geol. Soc. Am. Bull.* 85, 1721–1726.

Duchêne, S., Pupier, E., Le Carlier de Veslud, C., and Toplis, M. J. (2008). A 3D reconstruction of plagioclase crystals in a synthetic basalt. *Am. Mineral.* 93, 893–901. doi: 10.2138/am.2008.2679

Elliott, M. T., Cheadle, M. J., and Jerram, D. A. (1997). On the identification of textural equilibrium in rocks using dihedral angle measurements. *Geology* 25, 355–358.

Emeleus, C. H. (1997). *Geology of Rum and the Adjacent Islands. Memoir for 1:50 000 Geological Sheet 60 (Scotland)*. London: HM Stationery Office.

Emeleus, C. H., Cheadle, M. J., Hunter, R. H., Upton, B. G. J., and Wadsworth, W. J. (1996). "The rum layered suite," in *Layered Intrusions*, ed. R. G. Cawthorn, (Netherlands: Elsevier), 403–439. doi: 10.1016/s0167-2894(96)80014-5

Farr, R. S., Vukmanovic, Z., Holness, M. B., and Griffiths, E. (2018). Reconstructing grain-shape statistics from electron back-scatter diffraction microscopy. *Phys. Rev. Mater.* 2:073804. doi: 10.1103/PhysRevMaterials.2.073804

Gray, N. H., Philpotts, A. R., and Dickson, L. D. (2003). Quantitative measures of textural anisotropy resulting from magmatic compaction illustrated by a sample from the Palisades sill, New Jersey. *J. Volcanol. Geotherm. Res.* 121, 293–312. doi: 10.1016/s0377-0273(02)00463-8

Greenwood, R. C., Donaldson, C. H., and Emeleus, C. H. (1990). The contact zone of the Rhum ultrabasic intrusion; evidence of peridotite formation from magnesian magmas. *J. Geol. Soc.* 147, 209–212. doi: 10.1144/gsjgs.147.2.0209

Grout, F. F. (1918). Internal structures of igneous rocks: their significance and origin with special reference to the Duluth gabbro. *J. Geol.* 26, 439–458. doi: 10.1086/622605

Hamilton, M. A., Pearson, D. G., Thompson, R. N., Kelley, S. P., and Emeleus, C. H. (1998). Rapid eruption of Skye lavas inferred from precise U-Pb and Ar-Ar dating of the Rum and Cuillin plutonic complexes. *Nature* 394, 260–263. doi: 10.1038/28361

Heidelbach, F., Post, A., and Tullis, J. (2000). Crystallographic preferred orientation in albite samples deformed experimentally by dislocation and solution precipitation creep. *J. Struct. Geol.* 22, 1649–1661. doi: 10.1016/s0191-8141(00)00072-9

Hess, G. B. (1960). Stillwater igneous complex, Montana: a quantitative mineralogical study. *Geol. Soc. Am. Memoir* 80:230.

Higgins, M. D. (1991). The origin of laminated and massive anorthosite, Sept Iles layered intrusion, Quebec, Canada. *Contrib. Mineral. Petrol.* 106, 340–354. doi: 10.1007/bf00324562

Higgins, M. D. (1994). Numerical modelling of crystal shapes in thin sections: estimation of crystal habit and true size. *Am. Mineral.* 79, 113–119.

Higgins, M. D. (1998). Origin of anorthosite by textural coarsening: quantitative measurements of a natural sequence of textural development. *J. Petrol.* 39, 1307–1323. doi: 10.1093/petroj/39.7.1307

Higgins, M. D., and Chandrasekharam, D. (2007). Nature of sub-volcanic magma chambers, Deccan Province, India: evidence from quantitative textural analysis of plagioclase megacrysts in the Giant Plagioclase Basalts. *J. Petrol.* 48, 885–900. doi: 10.1093/petrology/egm005

Holness, M. B. (2007). Textural immaturity of cumulates as an indicator of magma chamber processes: infiltration and crystal accumulation in the rum Eastern Layered Intrusion. *J. Geol. Soc. Lond.* 164, 529–539. doi: 10.1144/0016-76492006-021

Holness, M. B. (2014). The effect of crystallization time on plagioclase grain shape. *Contrib. Mineral. Petrol.* 168:1076. doi: 10.1007/s00410-014-1076-5

Holness, M. B. (2015). Plagioclase growth rates control three-grain junction geometry in dolerites and gabbros. *J. Petrol.* 56, 2117–2144. doi: 10.1093/petrology/egv065

Holness, M. B., Anderson, A. T., Martin, V. M., Maclennan, J., Passmore, E., and Schwindinger, K. (2007a). Textures in partially solidified crystalline nodules: a window into the pore structure of slowly cooled mafic intrusions. *J. Petrol.* 48, 1243–1264. doi: 10.1093/petrology/egm016

Holness, M. B., Nielsen, T. F. D., and Tegner, C. (2007b). Textural maturity of cumulates: a record of chamber filling, liquidus assemblage, cooling rate and large-scale convection in mafic layered intrusions. *J. Petrol.* 48, 141–157. doi: 10.1093/petrology/egl057

Holness, M. B., Humphreys, M. C. S., Sides, R., Helz, R. T., and Tegner, C. (2012). Toward an understanding of disequilibrium dihedral angles in mafic rocks. *J. Geophys. Res.* 117:B06207.

Holness, M. B., Stock, M. J., and Geist, D. (2019). Magma chambers versus mush zones: constraining the architecture of sub-volcanic plumbing systems from microstructural analysis of crystalline enclaves. *Philos. Trans. R. Soc. A* 377:20180006. doi: 10.1098/rsta.2018.0006

Holness, M. B., Tegner, C., Namur, O., and Pilbeam, L. (2015). The earliest history of the skaergaard magma chamber: a textural and geochemical study of the cambridge drill core. *J. Petrol.* 56, 1199–1227. doi: 10.1093/petrology/egv034

Holness, M. B., Tegner, C., Nielsen, T. F. D., Stripp, G., and Morse, S. A. (2007c). A textural record of solidification and cooling in the Skaergaard intrusion, East Greenland. *J. Petrol.* 48, 2359–2377. doi: 10.1093/petrology/egm064

Holness, M. B., Vukmanovic, Z., and Mariani, E. (2017). Assessing the role of compaction in the formation of adcumulates: a microstructural perspective. *J. Petrol.* 58, 643–674.

Holness, M. B., and Winpenny, B. (2009). The Unit 12 allivalite, Eastern Layered Intrusion, Isle of Rum: a textural and geochemical study of an open-system magma chamber. *Geol. Magaz.* 146, 437–450. doi: 10.1017/s0016756808005797

Humphreys, M. C. S., and Holness, M. B. (2010). Melt-rich segregations in the Skaergaard Marginal Border Series: tearing of a vertical silicate mush. *Lithos* 119, 181–192. doi: 10.1016/j.lithos.2010.06.006

Hunter, R. H. (1996). Texture development in cumulate rocks. *Dev. Petrol.* 15, 77–101. doi: 10.1016/s0167-2894(96)80005-4

Ikeuye, K. K., and Smith, C. S. (1949). Studies of interface energies in some aluminium and copper alloys. *J. Miner. Metals Mater. Soc.* 1, 762–768. doi: 10.1007/BF03398934

Irvine, T. N. (1970). Heat transfer during solidification of layered intrusions. I. Sheets and sills. *Can. J. Earth Sci.* 7, 1031–1061. doi: 10.1139/e70-098

Irvine, T. N., Andersen, J. C. Ø, and Brooks, C. K. (1998). Included blocks (and blocks within blocks) in the Skaergaard intrusion: geological relations and the origins of rhythmic modally graded layers. *Geol. Soc. Am. Bull.* 110, 1398–1447.

Iso, Y., Cohen, C., and Koch, D. L. (1996). Orientation in simple shear flow of semi-dilute fiber suspensions 2. Highly elastic fluids. *J. Non Newt. Fluid Mech.* 62, 135–153. doi: 10.1016/0377-0257(95)01405-5

Jackson, E. D. (1961). "Primary textures and mineral associations in the ultramafic zone of the stillwater complex," in *Paper Presented at the Geological Survey Professional Paper 358*, (Washington: U.S Government Printing Office).

Jerram, D. A., Davis, G. R., Mock, A., Charrier, A., and Marsh, B. D. (2010). Quantifying 3D crystal populations, packing and layering in shallow intrusions: a case study from the Basement Sill, Dry Valleys, Antarctica. *Geosphere* 6, 537–548. doi: 10.1130/ges00538.1

Karykowski, B. T., and Maier, W. D. (2017). Microtextural characterisation of the Lower Zone in the western limb of the Bushveld Complex, South Africa: evidence for extensive melt migration within a sill complex. *Contrib. Mineral. Petrol.* 172:60. doi: 10.1007/s00410-017-1380-y

Kouchi, A., Tsuchiyama, A., and Sunagawa, I. (1986). Effect of stirring on crystallisation kinetics of basalt: texture and element partitioning. *Contrib. Mineral. Petrol.* 93, 429–438. doi: 10.1007/bf00371713

Kretz, R. (1966). Interpretation of the shape of mineral grains in metamorphic rocks. *J. Petrol.* 7, 68–94. doi: 10.1093/petrology/7.1.68

Kretz, R. (1994). *Metamorphic Crystallisation*. Chichester: John Wiley and Sons.

Latypov, R., Chistyakova, S., Barnes, S. J., and Hunt, E. J. (2017). Origin of platinum deposits in layered intrusions by in situ crystallisation: evidence from undercutting Merensky Reef of the Bushveld Complex. *J. Petrol.* 58, 715–762.

Lofgren, G. (1974). An experimental study of plagioclase crystal morphology: isothermal crystallization. *Am. J. Sci.* 274, 243–273. doi: 10.2475/ajs.274.3.243

Maaløe, S. (1976). The zoned plagioclase of the Skaergaard Intrusion, East Greenland. *J. Petrol.* 17, 398–419. doi: 10.1093/petrology/17.3.398

Mainprice, D., and Nicolas, A. (1989). Development of shape and lattice preferred orientations: application to the seismic anisotropy of the lower crust. *J. Struct. Geol.* 11, 175–189. doi: 10.1016/0191-8141(89)90042-4

Martin, D., Griffiths, R. W., and Campbell, I. H. (1987). Compositional and thermal convection in magma chambers. *Contrib. Mineral. Petrol.* 96, 465–475. doi: 10.1007/bf01166691

Mathison, C. I. (1987). Pyroxene oikocrysts in troctolitic cumulates – evidence for supercooled crystallization and postcumulus modification. *Contrib. Mineral. Petrol.* 97, 228–236. doi: 10.1007/bf00371242

McBirney, A. R., and Hunter, R. H. (1995). The cumulate paradigm reconsidered. *J. Geol.* 103, 114–122. doi: 10.1086/629727

McClurg, J. (1982). *Petrology and Evolution of the Northern Part of the Rhum Ultrabasic Complex*. Ph.D. thesis, University of Edinburgh, Edinburgh.

Meurer, W. P., and Boudreau, A. E. (1998). Compaction of Igneous cumulates Part II: compaction and the development of igneous foliations. *J. Geol.* 106, 293–304. doi: 10.1086/516023

Meurer, W. P., and Meurer, M. E. S. (2006). Using apatite to dispel the "trapped liquid" concept and to understand the loss of interstitial liquid by compaction in mafic cumulates: an example from the Stillwater Complex, Montana. *Contrib. Mineral. Petrol.* 151, 187–201. doi: 10.1007/s00410-005-0054-3

Miyazaki, T., Sueyoshi, K., and Hiraga, T. (2013). Olivine crystals align during diffusion creep of Earth's upper mantle. *Nature* 502, 321–326. doi: 10.1038/nature12570

Morgan, D. J., and Jerram, D. A. (2006). On estimating crystal shape for crystal size distribution analysis. *J. Volcanol. Geotherm. Res.* 154, 1–7. doi: 10.1016/j.jvolgeores.2005.09.016

Morse, S. A. (1986). Convection in aid of adcumulus growth. *J. Petrol.* 27, 1183–1214. doi: 10.1093/petrology/27.5.1183

Morse, S. A. (1988). Motion of crystals, solute, and heat in layered intrusions. *Can. Mineral.* 26, 209–224.

Nielsen, T. F. D. (2004). The shape and volume of the Skaergaard Intrusion, Greenland: implications for mass balance and bulk composition. *J. Petrol.* 45, 507–530. doi: 10.1093/petrology/egg092

O'Driscoll, B., Hargraves, R. B., Emeleus, C. H., Troll, V. R., Donaldson, C. H., and Reavy, R. J. (2007). Magmatic lineations inferred from anisotropy of magnetic susceptibility fabrics in Units 8, 9, and 10 of the Rum Eastern Layered Series, NW Scotland. *Lithos* 98, 27–44. doi: 10.1016/j.lithos.2007.01.009

Petford, N. (2009). Which effective viscosity? *Mineral. Magaz.* 73, 167–191. doi: 10.1180/minmag.2009.073.2.167

Petford, N., and Koenders, M. A. (2003). Shear-induced pressure changes and seepage phenomena in a deforming porous layer – I. *Geophys. J. Int.* 155, 857–869. doi: 10.1111/j.1365-246x.2003.02076.x

Petford, N., Koenders, M. A., and Clemens, J. D. (2020). Igneous differentiation by deformation. *Contrib. Min. Pet.* 175:45. doi: 10.1007/s00410-020-1674-3

Philpotts, A. R., Carroll, M. R., and Hill, J. M. (1996). Crystal-mush compaction and the origin of pegmatitic segregation sheets in a thick flood-basalt flow in the mesozoic hartford basin, connecticut. *J. Petrol.* 37, 811–836. doi: 10.1093/petrology/37.4.811

Philpotts, A. R., and Philpotts, D. E. (2005). Crystal-mush compaction in the Cohassett flood-basalt flow, Hanford, Washington. *J. Volcanol. Geotherm. Res.* 145, 192–206. doi: 10.1016/j.jvolgeores.2005.01.008

Renner, R., and Palacz, Z. (1987). Basaltic replenishment of the Rhum magma chamber - Evidence from Unit 14. *J. Geol. Soc. Lond.* 144, 961–970. doi: 10.1144/gsjgs.144.6.0961

Rust, B. R. (1972). Pebble orientation in fluvial sediments. *J. Sediment. Res.* 42, 384–388.

Sato, H. (1995). Textural difference between pahoehoe and aa lavas of Izu-Oshima volcano, Japan – an experimental study on population density of plagioclase. *J. Volcanol. Geotherm. Res.* 66, 101–113. doi: 10.1016/0377-0273(94)00055-l

Shea, T., and Hammer, J. E. (2013). Kinetics of cooling- and decompression-induced crystallsiation in hydrous mafic-intermediate magmas. *J. Volcanol. Geotherm. Res.* 260, 127–145. doi: 10.1016/j.jvolgeores.2013.04.018

Smith, J. V., and Brown, W. L. (1988). *Feldspar Minerals. Volume I: Crystal Structures, Physical, Chemical and Microtextural Properties*. Berlin: Springer-Verlag.

Svahnberg, H., and Piazolo, S. (2013). Interaction of chemical and physical processes during deformation at fluid-present conditions: a case study from

an anorthosite-leucogabbro deformed at amphibolite facies conditions. *Contrib. Mineral. Petrol.* 165, 543–562. doi: 10.1007/s00410-012-0822-9

Tait, S. R. (1984). *Fluid Dynamical Processes in The Formation of Layered Igneous Rocks*. Ph.D. thesis, University of Cambridge, Cambridge, MA.

Tait, S. R. (1985). Fluid dynamic and geochemical evolution of cyclic unit 10, Rhum, Eastern layered series. *Geol. Magaz.* 122, 469–484. doi: 10.1017/s0016756800035391

Upton, B. G. J., Parsons, I., Emeleus, C. H., and Hodson, M. E. (1996). "Layered alkaline igneous rocks of the Gardar Province, South Greenland," in *Layered Intrusions*, ed. R. G. Cawthorn, (Elsevier), 331–363. doi: 10.1016/s0167-2894(96)80012-1

Upton, B. G. J., Skovgaard, A. C., McClurg, J., Kirstein, L., Cheadle, M., Emeleus, C. H., et al. (2002). Picritic magmas and the Rum ultramafic complex, Scotland. *Geol. Magaz.* 139, 437–452. doi: 10.1017/s0016756802006684

Vernon, R. H. (1968). Microstructures of high-grade metamorphic rocks at Broken Hill, Australia. *J. Petrol.* 9, 1–22. doi: 10.1093/petrology/9.1.1

Vernon, R. H. (1970). Comparative grain-boundary studies of some basic and ultrabasic granulites, nodules and cumulates. *Scottish J. Geol.* 6, 337–351. doi: 10.1144/sjg06040337

Vukmanovic, Z., Holness, M. B., Monks, K., and Andersen, J. C. Ø (2018). The Skaergaard trough layering: sedimentation in a convecting magma chamber. *Contrib. Mineral. Petrol.* 173:43. doi: 10.1007/s00410-018-1466-1

Wager, L. R. (1963). The mechanism of adcumulus growth in the layered series of the Skaergaard intrusion. *Mineral. Soc. Am. Spec. Pap.* 1, 1–9.

Wager, L. R., and Brown, G. M. (1968). *Layered Igneous Rocks*. Edinburgh: Oliver and Boyd.

Wager, L. R., and Deer, W. A. (1939). *Geological Investigations in East Greenland Part III-The Petrology of the Skaergaard intrusion, Kangerdlussuaq, East Greenland*. Copenhagen: Meddelelser om Grønland.

Williams, S. R., and Philipse, A. P. (2003). Random packings of spheres and spherocylinders simulated by mechanical contraction. *Phys. Rev. E* 67:051301.

Yamamoto, S., and Matsuoka, T. (1996). Dynamic simulation of microstructure and rheology of fiber suspensions. *Polymer Eng. Sci.* 36, 2396–2403. doi: 10.1002/pen.10638

Young, I. M., and Donaldson, C. H. (1985). Formation of granular-textured layers and laminae within the Rhum crystal pile. *Geol. Magaz.* 122, 519–528. doi: 10.1017/s0016756800035433

Conflict of Interest: The authors declare that the research was conducted in the absence of any commercial or financial relationships that could be construed as a potential conflict of interest.